Continuum model of mixing and size segregation in a rotating cylinder: concentration-flow coupling and streak formation

D.V. Khakhar [a,*], Ashish V. Orpe [a], J.M. Ottino [b]

[a] Department of Chemical Engineering, Indian Institute of Technology-Bombay, Powai, Mumbai 400076, India
[b] Department of Chemical Engineering, McCormick School of Applied Science and Engineering, Northwestern University, Evanston, IL 60201, USA

Abstract

The effect of segregation and concentration-flow coupling on structure development in binary mixtures of different sized particles (S-systems) in a rotating cylinder is studied. The system is a prototype of tumbling mixers widely used in industry for mixing, coating and reaction. Experiments with S-systems have shown the formation of radial streaks of the small particles when the size ratio is large; however, an explanation of this phenomenon is not available. A continuum model is presented here for the flow in the layer using mass, momentum and species balance equations averaged across the layer. The stress is assumed to be a sum of the Bagnold stress and the Coulomb frictional stress; the temperature and total solids volume fraction are assumed to be uniform across the layer. We consider the case of a large difference in particle sizes so that segregation upon flow is instantaneous and a step concentration profile exists at all points in the flowing layer with the smaller particles forming the lower layer. The velocity profile is assumed to be piecewise linear with continuity of stress at the interface between the small and large particles. The model predicts the time varying velocity, layer thickness and concentration fields in the system. The predictions are compared to experimental flow visualization studies. Conditions for the formation of streaks are investigated.

Keywords: Granular mixing; Rotating cylinder; Size segregation

1. Introduction

Rapidly flowing granular materials in the *liquid-like state* are encountered in a number of industrial operations such as calcination in rotary kilns, mixing of pharmaceutical powders in tumbling mixers, and coating of seeds in pan coaters. Such rapid flows are also seen in natural systems such as sand dunes, avalanches and the rings of Saturn [1]. In all real systems the material is a mixture of particles of different sizes, and this has two important consequences: (i) the local fluidity (effective viscosity) is strongly influenced by the concentration of fine particles, and (ii) particles size segregate due to flow. The combination of these two effects can produce unique patterns, such as the radial streak pattern in a partially filled rotating cylinder with a square cross-section found by Hill et al. [2]. A model to predict such patterns has not yet been reported. Our objective here is to build a general *continuum* model to describe the mixing and segregation in a rotating cylinder taking into account the concentration flow coupling and to study the dynamics and pattern formation that are a consequence of this.

There are several alternative approaches for modelling granular flows: discrete models (particle dynamics, Monte Carlo simulations, and cellular automata) and continuum models (kinetic theory based models and their variants in which some parts may be empirical or evaluated from particle dynamics simulations). Particle dynamics simulations give a great wealth of detail about flows and mixing, however, they are limited to relatively small systems and simulations can be carried out for only small time periods of the flow. For example, *soft* particle dynamics are currently limited to systems containing 10^4 particles [3]. Cellular automata are particularly attractive because important underlying physical effects are clearly revealed in the formulation of the model. However, as of today, it appears that only continuum models are capable of quantitative predictions for large systems. Granular flows are typically far removed from traditional continua such as fluids and solids in which deformation length scales are several orders of magnitude larger than the molecules of the material. A question of particular relevance to the present study is “Can a continuum model describe particle size effects when the flowing layer is only a few particles deep?” Surprisingly, the answer is “yes”, and as we shall see below, continuum models are robust and give good predictions of granular phenomena in a variety of systems.

Flowing mixtures of particles of different sizes have been previously studied in a few different flow geometries, and we review these works below considering first the effect of size differences on flow, and then segregation due to size differences. A recent and more detailed review is given in Ottino and Khakhar [4].

The effect of size differences on flow was studied theoretically by Jenkins and Mancini [5] who obtained the transport equations for a binary mixture of nearly elastic, frictionless spheres based on the kinetic theory of hard spheres [6]. Predictions of the theory for a uniform mixture in shear flow showed that introducing smaller particles in the mixture significantly decreased the effective viscosity of the material. These results were in good agreement with the simulation results of Walton [7] for rough inelastic spheres. Higher order corrections to the transport theory have been obtained by Arnarson and Willits [8]. A theory for thin flowing layers has been proposed by Boutreux and deGennes [9]. The flux in this theory depends on the difference between the angle of the free surface and the static angle of repose. The flow is thus dominated by friction, and collisional viscosity effects do not appear explicitly.

Size segregation has been studied in three types of flowing systems: chute flows (free flow under gravity on an inclined surface), flows during heap formation, and rotating cylinder flows. In all three cases, segregation occurs due to the flow in a thin surface layer and thus the physics in the three cases is similar.

Savage and Lun [10] analyzed size segregation of a binary mixture of particles in a *chute flow* by means of experiment and theory. Experiments indicated that smaller particles percolate to the lower layers in the chute. They proposed a model for calculating the net percolation flux of the smaller particles, and the predicted distance along the chute for complete segregation of the mixture was in good agreement with experimental results. Hsiau and Hunt [11] studied segregation of a binary mixture in a gravity free shear flow due to a gradient in the *granular temperature* (the average kinetic energy of the fluctuation velocity of the particles) using the model of Jenkins and Mancini [5]. Small particles migrated to the higher temperature regions. Hirschfeld and Rapaport [12] carried out a computational study of chute flow of 2d Lennard–Jones particles in a gravitational field. Larger particles rose to the top of the layer as in the experiments of Savage and Lun [10]. Recently, Khakhar et al. [13] showed that the Jenkins and Mancini [5] theory predicts the equilibrium number fraction profiles for a binary mixture of inelastic smooth spheres in chute flow obtained from particle dynamics simulations. The theory, however, does not give good predictions for results of particle dynamics simulations for rough inelastic spheres in which inter-particle friction results in significant dissipation.

A mixture of particles poured to form a *2d heap* produces a pattern comprising streaks of the smaller particles. Drahun and Bridgwater [14] were the first to investigate this phenomenon. Recent experimental results are reported by Makse et al. [15] and Koeppe et al. [17]. A highly regular pattern with streaks of uniform thickness and of equal spacing between them is reported in these studies. Makse et al. [15] have proposed a cellular automaton model which gives patterns that are remarkably similar to the experimental results. In the model, rectangular particles (of different heights but the same width) are added one at a time at horizontal distances close to the peak. A particle “rolls” along the surface and comes to rest (always vertical) when the local slope is less than the maximum static angle of repose. If a particle “rolls” to the edge of the heap, the heap is said to be unstable and all particles “roll” until the local slope at each point on the surface is less than the minimum static angle of repose. In this model, coupling between the surface flow and concentration is only indirectly taken into account. The local angles and the heights of the particles are parameters of the system.

It is well known that in *rotating cylinders* smaller particles form a radial core while the larger particles migrate to the periphery in the rolling regime (which is observed at rotational speeds slightly higher than the avalanching regime). Prigozhin and Kalman [16] have proposed a model to predict this segregation using data extracted from heap formation experiments. A core with streaks is obtained when a binary mixture of particles with different angles of repose is taken [18]. Recently, Hill et al. [2] have found a new pattern—radial streaks—which is formed only for mixtures with a sufficiently large difference between the sizes of the components and when the mixer is slightly more than half-full. The effect appears to be very similar to the streak formation in 2d heap formation, and a qualitative explanation for streak formation given by Hill et al. [2] is based on the flow in the system which comprises a thin flowing surface layer ($-L < x < L$, see Fig. 1) with the remaining particles rotating as a fixed bed. Rotation results in a continuous input of particles into layer from the bed in the upper half of the layer ($-L < x < 0$), and a continuous output from the layer into the bed in the lower half of the layer ($0 < x < L$). The flow in the layer is faster when the concentration of the smaller particles is high because of their higher fluidity. Thus, a small streak entering the layer may be expected to lengthen due to acceleration of the flow. The degree of filling in the mixer is important because only a half-full mixer will

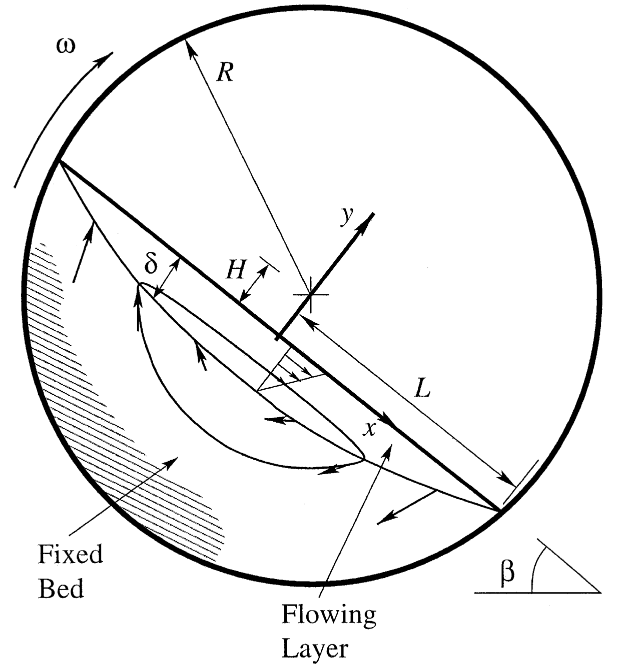

Fig. 1. Schematic view of the flow geometry. The coordinate system used in the analysis is shown.

allow a radial streak in the bed to enter the layer at once thus preserving its identity. When the mixer is less than half-full the streak reenters the layer gradually (since there is a non-zero angle between the streak and the bed–layer interface) as the mixer rotates and is dispersed.

The primary objective of the present work is to study the concentration flow coupling in flowing binary mixtures using a dynamic continuum model which incorporates the physics described above. The model is developed for a partially filled rotating cylinder with the objective of understanding the factors important for streak formation. Experimental studies of streak formation for binary mixtures of glass beads are also reported, and predictions of the model are compared to experimental results. The flow and transport model is described in the following section, together with computational details. Experimental details are given in Section 3, and the results and discussion in Section 4. The conclusions of the work are given in the final section.

2. Model equations

We consider the flow of a granular mixture in a rotating cylinder (Fig. 1). The fixed bed continuously feeds particles into the layer in the upper half ($x<0$) and absorbs particles from the layer in the lower half ($x>0$). The free surface is assumed to be nearly flat. The approach involves the use of macroscopic mass, momentum and species balance equations to obtain the time varying flow, layer thickness and concentration field in the system. The macroscopic balance equations are obtained by averaging the microscopic balance equations across the thickness of the layer. Constitutive models for the particle stress, diffusion and segregation fluxes are also required, in general. Particles with a large size difference (size ratio 1:3) are used in the experiments, and nearly complete segregation occurs rapidly. Here, as a simplification, we assume that segregation in the flowing layer is instantaneous. Thus, particles of different sizes cannot coexist in most of the flowing layer but separate into two layers with the smaller particles in the lower layer. This eliminates the need for a segregation flux constitutive equation. Small intermixing between the layers is incorporated by means of an empirical parameter, but this is assumed to have a negligible effect on the flow in the layer. Development of the model equations requires several additional assumptions, and these are given in the course of the derivation.

We develop here two versions of the dynamic model for flow, mixing and segregation in the cylinder. In the first version given below, the interface between the bed and flowing layer is assumed to be fixed in time (*static interface model*). In the second version, we generalize this model to allow the interface angle to change in a prescribed manner with composition of the flowing layer (*moving interface model*).

2.1. Static interface model

Consider the flow of a binary mixture of small (denoted by A) and large (denoted by B) particles flowing in the layer. The governing microscopic balance equations for the flow in the layer are given below. The continuity equation is:

$$\frac{\partial \rho}{\partial t}+\frac{\partial(\rho v_x)}{\partial x}+\frac{\partial(\rho v_y)}{\partial y}=0 \tag{1}$$

where ρ is the bulk density, and v_x and v_y are the velocity components. The momentum balance equation in the direction of the flow (x-component) is:

$$\frac{\partial(\rho v_x)}{\partial t}+\frac{\partial(\rho v_x^2)}{\partial x}+\frac{\partial(\rho v_x v_y)}{\partial y} = -\frac{\partial \tau_{xx}}{\partial x}-\frac{\partial \tau_{yx}}{\partial y}+\rho g \sin\beta \tag{2}$$

where β is the angle of the free surface. In this model, β is independent of x, and is taken to be equal to the value for the smaller particles, that is $\beta=\beta_{\mathrm{A}}$. In contrast, the free surface angle depends on position and time (i.e., $\beta(x,t)$) in the moving interface model. The particle pressure (P) does not vary in the x direction because the free surface is at a uniform pressure. Finally, the species balance equation for the smaller particles (denoted by A) is:

$$\frac{\partial \rho_A}{\partial t} + \frac{\partial(\rho_A v_{Ax})}{\partial x} + \frac{\partial(\rho_A v_{Ay})}{\partial y} = 0 \tag{3}$$

where ρ_A is the mass concentration of the smaller particles, and v_{Ax} and v_{Ay} are the components of the average velocity of the smaller particles. The mass concentration of the larger particles (ρ_B) is obtained from $\rho_B = \rho - \rho_A$.

Integrating Eqs. (1) to (3) across the layer (i.e., over the range $y \in (-\delta, 0)$), we get:

$$\frac{\partial \delta \langle \rho \rangle}{\partial t} + \frac{\partial(\delta \langle \rho v_x \rangle)}{\partial x} = \rho v_y|_{-\delta} \tag{4}$$

$$\frac{\partial(\delta \langle \rho v_x \rangle)}{\partial t} + \frac{\partial(\langle \rho v_x^2 \rangle)}{\partial x} = -\frac{\partial(\delta \langle \tau_{xx} \rangle)}{\partial x} + \tau_{yx}|_{-\delta} + \langle \rho \rangle g \delta \sin\beta + \rho v_x v_y|_{-\delta} \tag{5}$$

$$\frac{\partial(\delta \langle \rho_A \rangle)}{\partial t} + \frac{\partial(\delta \langle \rho_A v_{Ax} \rangle)}{\partial x} = \rho_A v_{Ay}|_{-\delta} \tag{6}$$

where the average across the layer is defined by:

$$\langle \oplus \rangle = \frac{1}{\delta} \int_{-\delta}^{0} \oplus \, \mathrm{d}y. \tag{7}$$

2.1.1. Assumptions

To simplify the above equations, we make several assumptions which are listed below.

(i) Constant ρ: The density is assumed to be uniform across the layer. This assumption is reasonable at low rotational speeds of the cylinder when the density of the flowing layer is only slightly less than the fixed bed value. The density is also assumed to be independent of concentrations; this is justified in the limit of complete segregation with the bulk density of each component close to the fixed bed value. The density of a mixture of two sizes would, in general, be higher than the pure component value.

(ii) Instantaneous segregation: Segregation is nearly instantaneous. The ratio of the particle sizes is large enough so that complete segregation exists in the flowing layer with the smaller particles occupying the lower part of layer.

(iii) Stress: The shear stress is a linear sum of the collisional (Bagnold) and frictional (Coulomb) stresses [19,20], that is:

$$\tau_{yx} = -c\lambda^2 \rho_p d^2 \left(\frac{\partial v_x}{\partial y}\right)^2 + \rho g y \cos\beta\mu \tag{8}$$

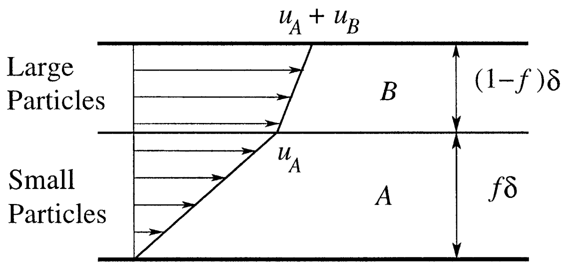

Fig. 2. Schematic view of the assumed shape of the velocity profile in the layer.

where ρ_p is the particle density, d the particle diameter and μ the coefficient of friction; c is a constant and λ is the linear packing density which is assumed to be constant. The higher fluidity of the smaller particles is implicit in the chosen stress equation ($\tau_{yx} \propto d^2$, see Eq. (8)). The coefficient of friction is estimated from $\mu = \tan\beta_s$, where β_s is the static angle of repose. Here we take value measured for the smaller particles, that is $\beta_s = \beta_{sA}$. Normal stress (τ_{xx}) variation in the flow direction (x direction) is neglected.

(iv) Linear velocity profile: The velocity profile is piecewise linear. Since the flowing layer is completely segregated, there is a layered shear flow of the particles with the smaller particles in the lower layer. Experiments for pure component systems show a nearly linear velocity profile in the layer with no slip at the bed–layer interface [21–23]. We extrapolate this result to the case of two adjacent flowing layers, each a pure component layer (Fig. 2). The velocity profile is thus:

$$v_x = u_A \left(\frac{y+\delta}{f\delta}\right) \qquad y \in (-\delta, -(1-f)\delta) \tag{9}$$

$$v_x = u_A + u_B \left(1 + \frac{y}{(1-f)\delta}\right) \qquad y \in (-(1-f)\delta, 0)$$

where u_A is the maximum velocity in the small particle (bottom) layer, and ($u_A + u_B$) is the maximum velocity in the large particle (top) layer. The fraction of the layer occupied by the smaller particles is f. The velocity profile in Eq. (9) is continuous across the interface.

The fraction of the layer that is occupied by the smaller particles (f) is related to the local mass density of the smaller particles by:

$$f = \langle \rho_A \rangle / \rho. \tag{10}$$

Further, the velocities u_A and u_B are related to each by the continuity of stress at interface between the small particle layer and the large particle layer:

$$\tau_{yx}^A = \tau_{yx}^B \quad \text{at } y = -(1-f)\delta. \tag{11}$$

Substituting for the stress and taking $\mu_A \approx \mu_B$, $c_A = c_B$, $\lambda_A = \lambda_B$ and the densities of the two particles to be the same, we get:

$$u_B = u_A\left(\frac{d_A}{d_B}\right)\frac{1-f}{f}. \tag{12}$$

If we take μ_A and μ_B to be different, then μ_B is given by a somewhat more complicated expression:

$$u_B = \left[u_A^2\left(\frac{d_A}{d_B}\right)^2\left(\frac{1-f}{f}\right)^2 + \frac{\rho g(1-f)^3\delta^3\cos\beta(\mu_A - \mu_B)}{c\lambda^2\rho_p}\right]^{1/2}. \tag{13}$$

In the results reported here, we use Eq. (12) as a simplification, with the assumption $\mu_A \approx \mu_B$.

2.1.2. Simplified governing equations

With the above assumptions, the unknown variables are $u_A(x,t)$, and $\delta(x,t)$. Thus, with the three governing equations we have a closed system that can be solved with appropriate boundary conditions. The averaged continuity equation, using the assumption of a constant bulk density (ρ), reduces to:

$$\frac{\partial\delta}{\partial t} + \frac{\partial(\delta\langle v_x\rangle)}{\partial x} = v_y|_{-\delta}. \tag{14}$$

The average velocity in the layer obtained from the assumed velocity profile is:

$$\langle v_x\rangle = u_A\left(1-\frac{f}{2}\right) + u_B\frac{1-f}{2}. \tag{15}$$

Assuming that the bed–layer interface remains static (static interface model) and that the layer is thin ($\delta/L \ll 1$), the velocity of particles into and out of the layer is:

$$v_y|_{-\delta} = -\omega x. \tag{16}$$

Thus, the continuity equation becomes:

$$\frac{\partial\delta}{\partial t} = -\frac{\partial(\delta\langle v_x\rangle)}{\partial x} - \omega x. \tag{17}$$

The averaged momentum balance equation, using the assumptions of a constant bulk density (ρ) and $v_x(-\delta) = 0$, and neglecting the variation of normal stress along the layer, reduces to:

$$\frac{\partial(\delta\langle v_x\rangle)}{\partial t} + \frac{\partial(\delta\langle v_x^2\rangle)}{\partial x} = \frac{1}{\rho}\tau_{yx}\Big|_{-\delta} + g\delta\sin\beta. \tag{18}$$

The mean square velocity using the assumed velocity profile is given by:

$$\langle v_x^2\rangle = u_A^2\left(1-\frac{2f}{3}\right) + u_A u_B(1-f) + u_B^2\frac{1-f}{3} \tag{19}$$

and the shear stress at the bed–layer interface is:

$$\frac{1}{\rho}\tau_{yx}\Big|_{-\delta} = \begin{cases} -c\lambda^2\dfrac{\rho_p}{\rho}d_A^2\left(\dfrac{u_A}{f\delta}\right)^2 - g\delta\mu_A\cos\beta & f \geq \varepsilon \\ -c\lambda^2\dfrac{\rho_p}{\rho}d_B^2\left(\dfrac{u_B}{(1-f)\delta}\right)^2 - g\delta\mu_B\cos\beta & f < \varepsilon. \end{cases} \tag{20}$$

For complete segregation, we must have $\varepsilon = 0$. Here we take ε to be a small number ($\varepsilon \sim 10^{-3}$) with the physical significance that when the concentration of the smaller particles is less than ε, the mixture behaves as pure B (large particles). As we shall see, changing ε by an order of magnitude has no effect on the results.

The species balance equation on assumption of a constant bulk density across the layer becomes:

$$\frac{\partial(\delta f)}{\partial t} + \frac{\partial(\delta\langle v_{Ax}\rangle)}{\partial x} = \frac{\rho_A}{\rho}v_{Ay}\Big|_{-\delta}. \tag{21}$$

The average velocity of the smaller particles obtained from the assumed velocity profile is:

$$\langle v_{Ax}\rangle = \frac{u_A f}{2} \quad f > 0 \tag{22}$$

and the input term (for $x < 0$) is:

$$\frac{\rho_A}{\rho}v_{Ay}\Big|_{-\delta} = -\omega x f_b|_{-\delta} \tag{23}$$

where f_b is the volume fraction of the smaller particles in the bed.

The output term in Eq. (21) (for $x > 0$) is given by:

$$\frac{\rho_A}{\rho}v_{Ay}\Big|_{-\delta} = -\omega x f|_{-\delta}. \tag{24}$$

If there was no mixing in the layer the composition at the interface ($f|_{-\delta}$) could be either 0 (purely large particles) or 1 (purely small particles). Here we assume a small mixed region of thickness, δ_m, between the pure layers of large and small particles, in which the composition varies linearly from $f = 0$ to $f = 1$. As mentioned previously, δ_m

is taken to be small so that the flow remains unaffected. In this case, the number fraction at the bed–layer interface is obtained as:

$$f|_{-\delta} = \begin{cases} 1 & \text{if } f\delta \geq \delta_\mathrm{m} \\ f\delta/\delta_\mathrm{m} & \text{if } f\delta < \delta_\mathrm{m} \text{ and } \delta > \delta_\mathrm{m} \\ f & \text{if } \delta \leq \delta_\mathrm{m}. \end{cases} \qquad (25)$$

Thus, if the thickness of the layer of the small particles $(f\delta)$ is larger than the thickness of the mixed region (δ_m) only small particles enter the bed, whereas if the thickness of the mixed region is greater than the total layer thickness, the composition of the particles entering the bed is equal to the average composition in the layer. By means of this empirical model we can tune the mixing in the system. The value of δ_m depends, in general, on a balance between local diffusion and segregation rates. Here, however, we take it to be model parameter.

The final component of the model relates to the no flux condition at $x = L$ (Fig. 1) which corresponds to the cylinder surface. This condition cannot be satisfied, in general, since the τ_{xx} term in the momentum balance equation is neglected. For steady flow, the boundary condition is satisfied due to mass conservation, however, in the dynamic case some particles may leak across the boundary. To conserve mass in our model, we treat the boundary as a reflective surface and map the particles that cross the boundary to the lower part of the layer $(x > 0)$, and this appears as a flux into the layer. The mapped flux is assumed to vary linearly with distance with the maximum value at the wall. The magnitude of this flux is small and does not significantly affect the flow, however, if it is not taken into account, significant loss of mass occurs over long times.

Eqs. (17), (18) and (21) together with Eq. (12) give four equations to calculate the four variables: u_A, u_B, δ and f in the layer as a function of time. In addition, the time varying composition in the bed $(f_\mathrm{b}(x,y,t))$ must be computed, taking into account the particles entering from the layer in the region $x < 0$ and solid body rotation about the axis. This completes the definition of the static interface model.

2.2. Moving interface model

Experimental observations (which are discussed later) indicate that the free surface does not remain fixed, but the slope of the free surface varies locally depending on the composition of the layer. We modify the model described in the previous sub-section to take this fact into account in a simple way. The layer is divided into three segments: a central segment of length $2x_\mathrm{c}$ with a fixed angle and an upper and a lower segment that are hinged at the ends of the fixed segment and may rotate (Fig. 3). In general, $x_\mathrm{c} \ll L$ in the context of the model. If the average composition in the upper or lower segment is greater than a critical value (f_c), the equilibrium free surface angle (β_eq) is taken to be the dynamic angle of repose of the smaller beads (β_A) else it is the dynamic angle of repose of the larger beads (β_B). Finally, if the current angle of a segment is less than the equilibrium value, the angle increases as the segment rotates at a constant rotational speed ω_i, whereas if the angle is greater than the equilibrium value at that time the angle decreases at the same rate. The rate of change of the free surface angles introduces two additional differential equations:

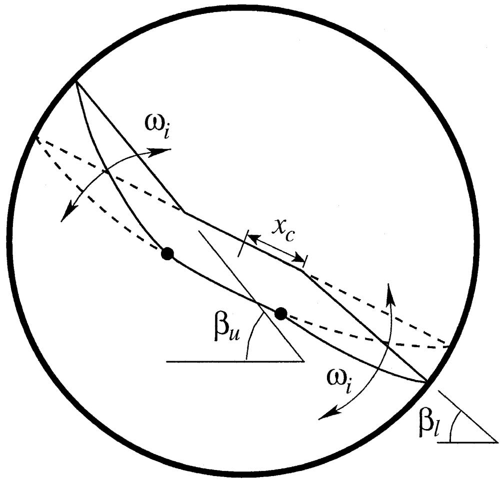

Fig. 3. Figure showing how the surface angles change in the moving interface model.

$$\frac{\mathrm{d}\beta_\mathrm{u}}{\mathrm{d}t} = \begin{cases} \omega_\mathrm{i} & \text{if } \beta_\mathrm{u} < \beta_\mathrm{eq} \\ -\omega_\mathrm{i} & \text{if } \beta_\mathrm{u} > \beta_\mathrm{eq} \end{cases}$$

$$\frac{\mathrm{d}\beta_\mathrm{l}}{\mathrm{d}t} = \begin{cases} \omega_\mathrm{i} & \text{if } \beta_\mathrm{l} < \beta_\mathrm{eq} \\ -\omega_\mathrm{i} & \text{if } \beta_\mathrm{l} > \beta_\mathrm{eq} \end{cases} \qquad (26)$$

where β_u and β_l are the free surface angles of the upper and lower segments, respectively (Fig. 3).

The particles in the bed rotate at a fixed rotational speed, ω, thus producing flux of particles into (or out of) the flowing layer. The motion of the interface results in an additional (positive or negative) contribution to the flux of particles into layer. The velocity relative to the moving bed layer interface must thus be considered, and this can be taken into account easily by replacing the rotational speed of the cylinder by an effective rotational speed given by:

$$\omega_\mathrm{eff} = \omega - |x - x_\mathrm{c}|\omega_\mathrm{i}/(x^2 + H^2)^{1/2}, \qquad (27)$$

in the governing equations of the static interface model. The expansion and contraction of the bed as a consequence of the motion of the interface is also taken into account in the model.

2.3. Numerical solution

Defining the variables $q = \delta\langle v_x\rangle$, $q_m = \delta\langle v_x^2\rangle$, $q_A = \delta\langle v_{Ax}\rangle$ and $C = f\delta$, the governing equations for the problem reduce to:

$$\frac{\partial\delta}{\partial t} = -\frac{\partial q}{\partial x} - \omega_{eff}\, x \tag{28}$$

$$\frac{\partial q}{\partial t} = -\frac{\partial q_m}{\partial x} + \frac{1}{\rho}\tau_{yx}\Big|_{-\delta} + g\delta\sin\beta \tag{29}$$

$$\frac{\partial C}{\partial t} = -\frac{\partial q_A}{\partial x} + \frac{\rho_A}{\rho}\Big|_{-\delta}\omega_{eff}\, x. \tag{30}$$

The solution is carried out using the finite difference method using a forward-time and backward-space difference scheme. The layer is discretized in the x direction, and the initial values of the average velocities (u_A, u_B) the layer thickness (δ) and the fraction of layer occupied by the smaller particles (f) at each grid point are used to compute q, q_m, q_A and c. The values of δ, q and C are computed at a particular time step based on values at the previous time step using the finite difference equations. The average velocities (u_A, u_B) and f and subsequently q, q_m, q_A and C are computed based on the new values, and the process is repeated. The bed concentration values are stored in a matrix that is updated after a time interval $\Delta t = \pi/400\omega$; the integration time step $(\mathrm{d}t)$ is smaller by two orders of magnitude $(\mathrm{d}t = 10^{-4}/\omega)$. The updating procedure involves moving all positions by an angle $\Delta\omega t$, and adding or removing elements at the interface depending on the motion of the interface.

3. Experimental details

Flow visualization experiments were carried out to study the conditions for and the dynamics of streak formation in a rotating cylinder. A few of the parameters required for the model such as the static and dynamic angles of repose and layer thicknesses during flow were also measured by image analysis.

The quasi 2d rotating cylinder (16 cm radius and 1 cm thickness) was rotated at a fixed rotational speed using a stepper motor. The front and rear plates of the cylinder were made from transparent PMMA. Glass beads of diameter 3, 2 and 1 mm were used in the experiments and were coloured using permanent marker inks (Camlin).

All experiments were carried out with 50% vol/vol mixtures of small and large beads. Two different size ratios $(r_S = d_A/d_B)$ for the S-systems were used: $r_S = 1/3$ and $r_S = 2/3$. The cylinder was filled to a specified volume fraction (usually 0.5), and rotated at a high angular speed (10 rpm). No streaks were formed at this speed and the particles were radially segregated with the smaller particles forming the inner core. This ensured a uniform initial condition in all the experiments. The rotation of the cylinder was then stopped and restarted at the desired rotational speed. Photographs were taken of the initial state and after intervals of one revolution of the mixer to study the dynamics of band formation. Once streaks were formed, photographs were taken at different times to sample the different compositions of the layer which changed as the mixer rotated. The free surface angles (dynamic angles of repose) were measured from these photographs, with a plumbline serving to mark the vertical direction. A few photographs were taken at long exposure times (1/2 s) to obtain streaklines. The layer thicknesses were obtained from these photographs for different layer compositions.

4. Results and discussion

4.1. Experimental results

We first present the results of a study of streak formation as a function of the system parameters (particle size ratio, rotational speed and degree of filling), and then give the results of the angles of repose and layer thickness measurements.

Fig. 4 shows the dynamics of streak formation for different cylinder rotational speeds, for a mixture of 3 mm (dark) and 1 mm (light) beads $(r_S = 1/3)$. The starting point in all three cases is a radially segregated core of small particles formed at high rotational speeds. The lowest rotational speed (0.75 rpm) initially results in sharper interface between the small and large particle regions, however, the interface becomes jagged after one revolution (Fig. 4). This marks the start of the streaks which grow with every revolution, until the streaks composed of the smaller particles penetrate to the cylinder periphery, at the end of five revolutions.

At a higher rotational speed (1.5 rpm), the behavior is similar, however, the streaks do not grow to reach the cylinder periphery (Fig. 4). At an even higher rotational speed (2.25 rpm), no streak formation is evident up to five revolutions.

Increasing rotation times does not result in any qualitative changes in the structure in either of the three cases. Streaks, once formed, maintain their identity for relatively long periods. On a much longer time scale, however, the streaks are dynamic and two neighboring streaks may merge or a new streak may be generated in the gap between two streaks. The dynamics appear to be complex and irregular, and seem to be influenced by the distance between neighboring streaks. A detailed study of these long-term dynamics was not carried out, however. Rotation for long times (20 min) did not produce streaks in the two cases rotated at higher speeds (1.5 and 2.25 rpm).

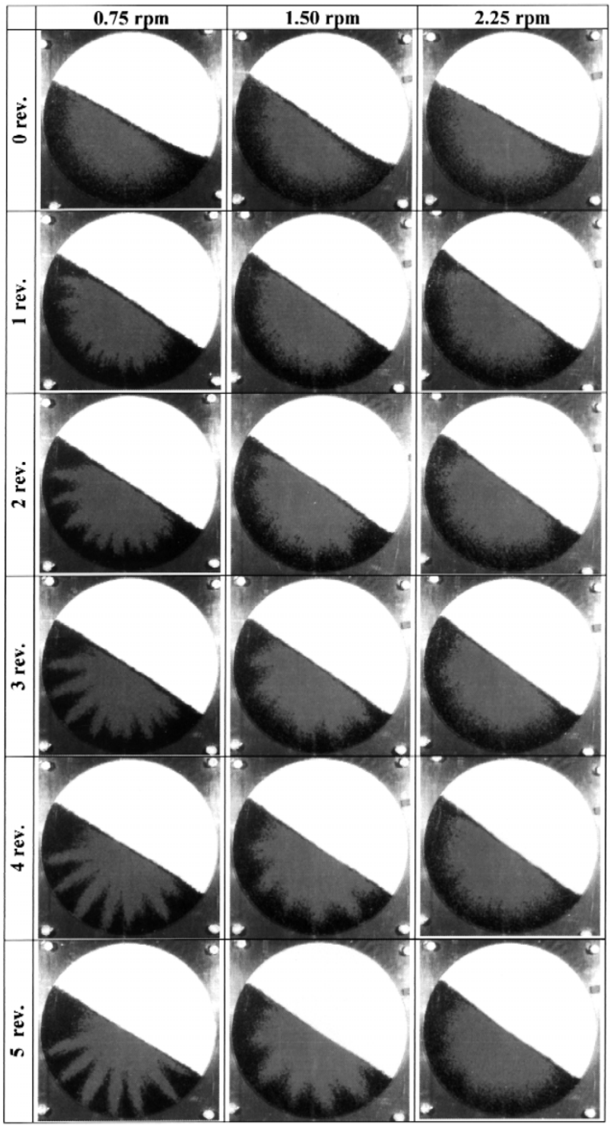

Fig. 4. Experimental photographs showing the dynamics of streak formation at different rotational speeds. A 50% vol/vol mixture of 3 mm (dark) and 1 mm (light) beads are used.

Fig. 5 shows the pattern formed after five revolutions for two different cases: in one, the degree of filling is reduced to 25% and in the second, a 50% vol/vol mixture of 3 and 2 mm beads is used ($r_S = 2/3$). Reducing the fill level eliminates the streaks, while increasing the particle size ratio produces partial streaks.

While the effect of fill fraction was previously known [2], the results concerning the dependence of pattern formation on rotational speed and size ratio are new. The results are, however, consistent with the mechanism described in the first section. Increased rotational speeds improve mixing in the layer, thus concentration fluctuations that produce nascent streaks are smoothed out. Smaller differences in sizes of particles in the mixture result in smaller change in fluidity with addition of the small particles, thus the instability is suppressed.

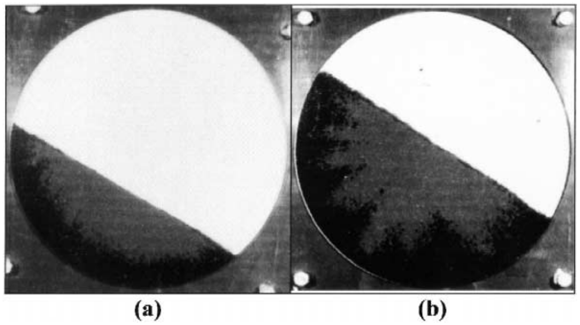

Fig. 5. Pattern formed after five revolutions for 50% vol/vol mixture of large (dark) and small (light) beads for a cylinder rotational speed of 0.75 rpm. (a) Mixture of 3- and 1-mm beads at a fill fraction of 0.25. (b) Mixture of 3- and 2-mm beads at a fill fraction of 0.5.

Consider next the details of the flow after the streaks are formed. Fig. 6(a) shows a streamline photograph of the flow in the layer of the 3 and 1 mm mixture ($r_S = 1/3$) at 0.75 rpm when both light coloured and dark coloured particles are co-flowing in at least part of the layer. The segregation between the two is nearly complete in agreement with the model assumption. Fig. 6(b) shows a snapshot of a radial streak of small particles just entering the layer in the top half and beginning to cascade down. Notice that the streak enters the layer all at once and the entire top half of the layer ($x < 0$) becomes filled with the smaller particles (light coloured). The small particles have not reached the lower half of layer ($x < 0$) which is almost fully dark. Due to differences in composition along the layer, the difference in the dynamic angle of repose is clearly evident: the smaller particles have a smaller dynamic angle of repose as compared to the larger particles. The difference between the two is significant (Table 1). Thus, the free surface is dynamic with local angles increasing and decreasing depending on the local composition.

Similar streakline photographs are used to obtain the layer thicknesses of the light coloured and dark coloured layers which are useful for the estimation of the parameter

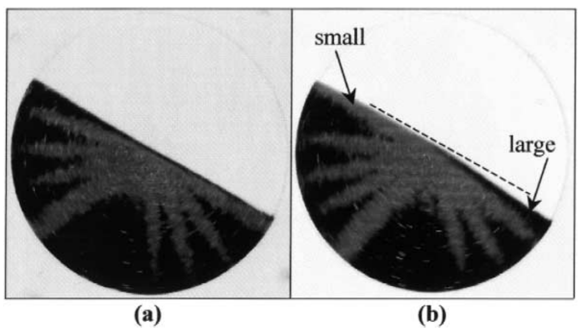

Fig. 6. Streakline photographs for a 50 % vol/vol mixture of 3 mm (dark) and 1 mm (light) glass beads for a cylinder rotational speed of 0.75 rpm. (a) Co-flowing particles in the lower part of the layer show nearly complete segregation. (b) Free surface angle is significantly smaller when the smaller (light) particles fill the layer relative to when the larger (dark) particles fill the layer.

Table 1
Measured static (β_{sA}, β_{sB}) and dynamic (β_A, β_B) angles of repose for small (A) and large (B) particles in a cylinder of diameter 32 cm. The dynamic angles are measured at a rotational speed of 0.75 rpm

	Angle of repose (°)	
	Small particles (A)	Large particles (B)
Static (β_s)	25.7	29.8
Dynamic (β)	29.2	33.5

c in the stress equation (Eq. (20)). Total layer thicknesses in the range $0.07R$ to $0.09R$ were obtained. The static angles of repose were measured for mixers half-filled with pure components, and are given in Table 1.

4.2. Computational results

The model presented here is a generalization of the steady state model given Khakhar et al. [24], and at steady state, and for a single component system ($f = 1$) both should give the same result. Fig. 7 shows a comparison between the two models for parameters corresponding to 3 mm glass beads and a cylinder angular speed of 1 rpm. The free surface is held fixed in the dynamic model in this case (static interface model, $\omega_i = 0$). There is close agreement between the predictions of the two for the mean velocity ($u = u_A/2$) and layer thickness profiles. In case of the dynamic model the results are plotted after a sufficient time so as to achieve a steady state. This occurs very quickly (0.02 revolutions) as is evident from the results in Fig. 8, which show the variation of the scaled mean velocity and the volume flux at the mid point of the layer ($x = 0$) for the system starting from rest. The asymptotic value of the volume flux, $q(0)/\omega R^2 = 1/2$, is also in agreement with the predictions of previous models for single component steady flows [20,24].

4.2.1. Static interface model

Consider next the evolution of a radial streak when the interface is held fixed (i.e., $\omega_i = 0$). The initial configuration in this case (Fig. 9) is taken to be a segregated core with a single radial streak. The parameters used in the computations correspond to a mixture of 3 and 1 mm glass beads for a cylinder rotational speed of 0.75 rpm. Since the free surface angle remains fixed, only one set of the angles of repose can be used in the model. Here the measured values of the angles of repose corresponding to the small particles are used, and the parameter c (Eq. (20)) is adjusted to obtain layer thicknesses of roughly the same magnitude as those experimentally obtained. A second adjustable parameter of the model is δ_m, the thickness of

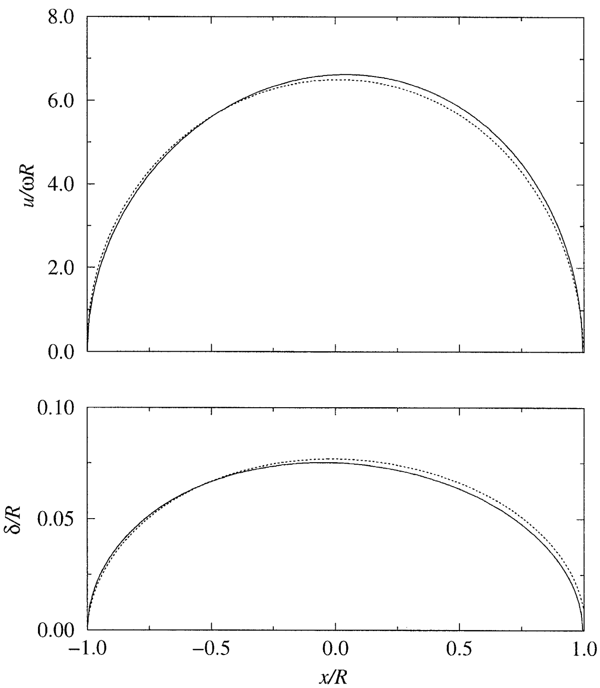

Fig. 7. Comparison of the scaled mean velocity ($u/\omega R$) and layer thickness (δ/R) with scaled distance along the layer (x/R) at steady state of a single component system ($f = 1$). The solid lines are predictions of the dynamic model and the dotted lines are the predictions of the steady state model of Khakhar et al. [24].

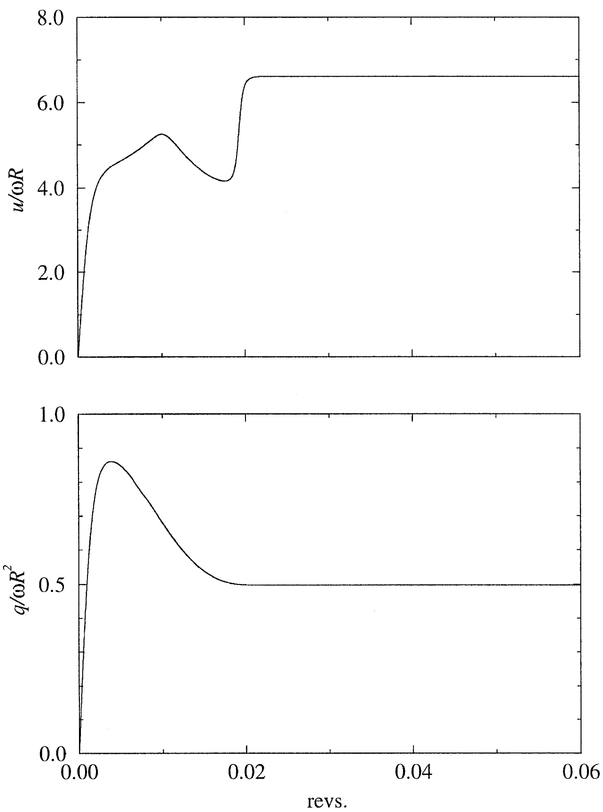

Fig. 8. Dynamic variation of the scaled mean velocity ($u/\omega R$) and volume flux ($q/\omega R^2$) with rotation at the mid point of the layer ($x = 0$) for a pure system starting from rest. The time to reach steady state is about 0.02 revolutions. Notice that the asymptotic scaled volume flux is $q/\omega R^2 = 1/2$ as predicted by theories of Rajchenbach [20] and Khakhar et al. [24].

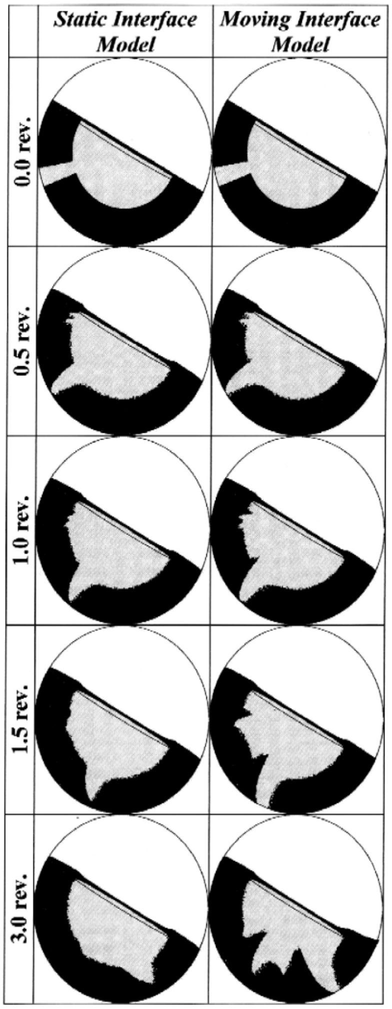

Fig. 9. Computational results showing the evolution of a preformed radial streak with rotation of the cylinder. The parameters used correspond to a mixture of 3- and 1-mm beads, and the cylinder rotational speed is 0.75 rpm. Left: Static interface model. Notice that the streak shortens slightly and spreads with rotation. Right: Moving interface model. The streak is preserved.

the mixed region in the flowing layer. Here we assume $\delta_m = 0.01R \approx d_B/2$, that is, the thickness of the mixed region is of the order of magnitude of the radius of the large particles. This gives simulation results which are qualitatively similar to experiments. The value may be reasonable considering the low rotational speed used ($\omega =$ 0.75 rpm), which is just beyond the avalanching regime.

Fig. 9 shows the computational results in terms of the pattern evolution with rotation. The results indicate that the streak shortens with time and is not preserved by the flow. The variation of the scaled velocities ($u_A/\omega R$, $u_B/\omega R$) and volume flux ($q/\omega R^2$) at the mid point of the layer ($x = 0$) with rotation is shown in Fig. 10. There is a sharp increase in the velocity of the smaller particles (A) when the streak enters the layer, and the velocity of the larger particles (B) falls briefly to zero which corresponds to the layer completely filled with the smaller particles. The volume flux first increases then decreases with rotation as the streak passes through. The increase in flux occurs because the fluidity of the smaller particles is greater and this results in a faster flow and thus a thinner layer. The excess flow is due to the material that must flow out, in addition to the steady input, to make the layer thinner. Once the layer is completely filled with the smaller particles nearly steady state flow is achieved as indicated by the asymptotic value of the flux ($q(0)/\omega R^2 = 1/2$). Later as the large particles begin entering the layer, the flow slows and the layer thickens resulting in a lower flux at the center of the layer.

The minor oscillations in the curves in Fig. 10 do not appear to be computational artifacts since identical results are obtained when the integration time step is reduced by a factor of 2 (Fig. 10). Reducing the value of the parameter ε (Eq. (20)) by order of magnitude also has no effect as shown in Fig. 10.

These computations seem to indicate that simply taking into account the contribution of more rapid flow of the smaller particles in the layer may not be sufficient to produce and sustain radial streaks. In fact, computations using this model for widely different parameter values

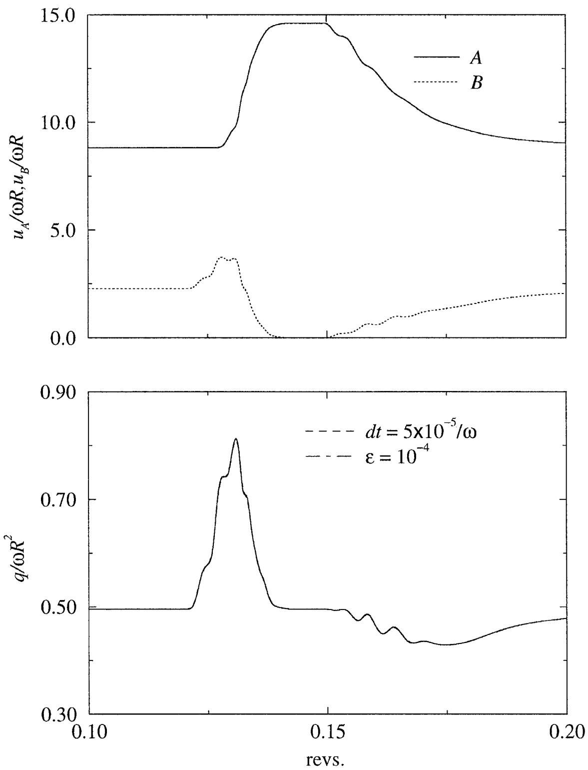

Fig. 10. Time variation of the scaled velocities ($u_A/\omega r$, $u_B/\omega r$) and volume flux ($q/\omega R^2$) at the mid point of the layer ($x = 0$) as a streak of the smaller particles (A) passes through the layer for the fixed interface model. The computations correspond to the initial condition and parameters of Fig. 9. The velocity of the smaller particles and the volume flux increases when the streak enters the layer. Graphs of the volume flux computed with an integration step (dt) smaller by a factor of 2, and with ε smaller by a factor of 10 exactly superimpose on the solid line.

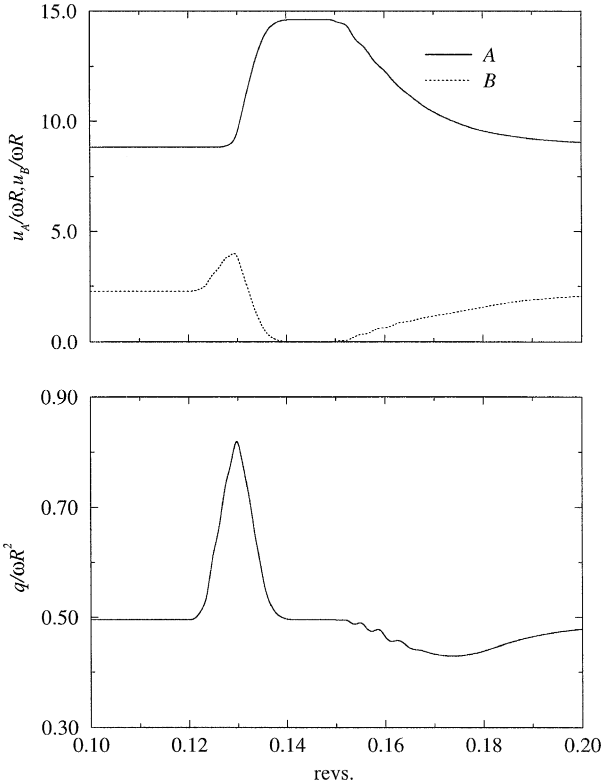

Fig. 11. Variation of the scaled velocities ($u_A/\omega r$, $u_B/\omega r$) and volume flux ($q/\omega R^2$) with cylinder rotation when a streak of the smaller particles (A) passes through the layer for the moving interface model. The computations correspond to the initial condition and parameters of Fig. 9.

yielded no streaks starting from a radially segregated core (corresponding to the experimental initial condition). Small changes in the angle of the free surface appear to have an important role in the process, and we examine this next.

4.2.2. Moving interface model

The moving interface model contains three additional parameters: ω_i, the rotational speed of the interface, x_c, the size of the static segment of the interface and f_c, the critical composition. Independent values of these parameters are not available, hence we assume physically reasonable values in the computations. Experimental results indicate that x_c may be small (see, for example, Fig. 6(b)), and here we take $x_c = 0.05R$. The critical concentration, f_c, has a very significant effect on streak formation for the following reasons. The average composition in each segment in the layer depends on the fraction of small beads in the cylinder, and f_c must be close to this average value in the layer. If f_c is much larger or much smaller than the average value, the interface angles remain constant and equal to those for the larger or smaller particles, respectively. Thus, in these limiting cases, the model reduces by default to the static interface model and no streaks are seen. Here we tune f_c so that it is close to the average value so that concentration fluctuations result in time variation of the surface angles ($\beta_u(t), \beta_l(t)$). The interface rotational speed (ω_i) does not qualitatively affect the pattern formation process, although it has a significant impact on the number and thickness of streaks formed and on the rate of streak growth. As a first estimate we may assume ω_i to be of the same order of magnitude of the cylinder rotational speed (ω). In all the computations reported here, we take $\omega_i = 0.3\omega$ since it gives streaks that qualitatively resemble the experimentally obtained streaks.

The measured dynamic angles of repose (Table 1) were used in the computations. As mentioned previously, the same value of the static angle of repose for the smaller and larger particles ($\beta_{sB} = \beta_{sA} = 25.7°$) was used.

Fig. 9 shows the evolution of a constructed radial streak as predicted by the moving interface model along side the results of the static interface model. The patterns are nearly identical until the end of the first revolution. The streak in the moving interface model, however, survives the flow and additional smaller streaks are produced in the wake of the larger streak. The contrast in the patterns obtained after three revolutions from the fixed interface and moving interface models is clear. Further rotation (five revolutions) results in complete shrinkage of the remnant of the streak in the fixed interface model, whereas the streak survives in case of the moving interface model.

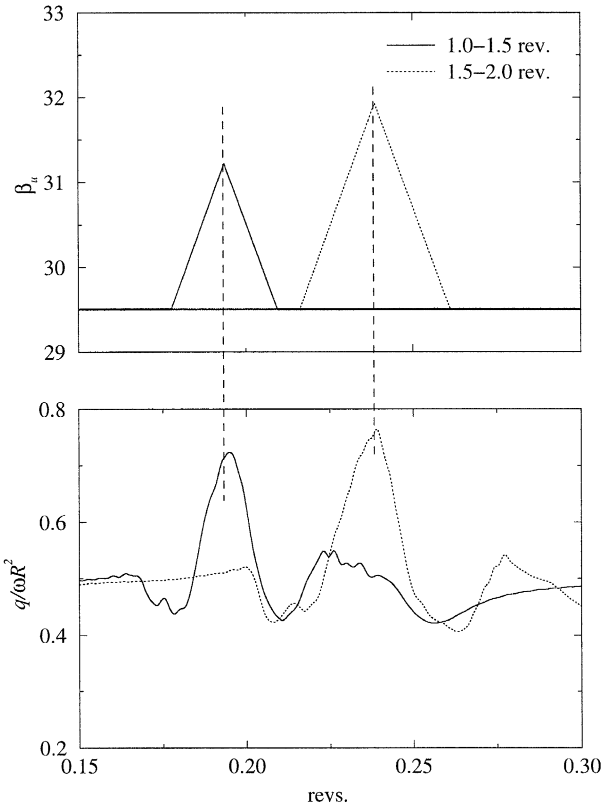

Fig. 12. Variation of the upper surface angle (β_u) and the scaled volume flux ($q(0)/\omega R^2$) with cylinder rotation when the streak of the smaller particles (A) repeatedly passes through the layer computed using the moving interface model. The computations correspond to the initial condition and parameters of Fig. 9.

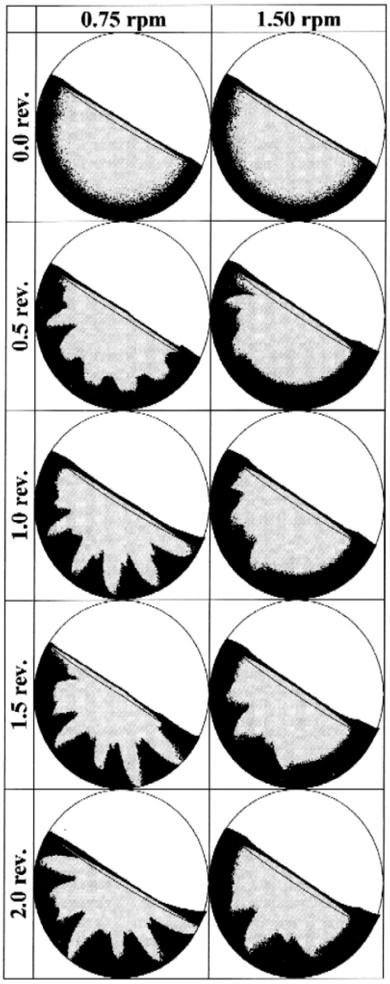

Fig. 13. Computed patterns showing the dynamics of streak formation at different rotational speeds.

The dynamic variation of scaled velocities ($u_A(0)/\omega R$, $u_B(0)/\omega R$) and volume flux ($q(0)/\omega R^2$) at the mid point of the layer ($x = 0$) are shown in Fig. 11 as the streak passes through the layer for the first time. The behavior is nearly identical to the static interface case; this is not surprising considering the similarity of the initial patterns.

How does the motion of the interface act to preserve the streak? A possible answer to this question is revealed in Fig. 12 which shows the time variation of the upper angle of the free surface (β_u) and the mid layer flux ($q(0)/\omega R^2$). The time variation over intervals of duration $1/2$ revolution are superimposed. Until the end of the first revolution there is no motion of the upper part of the interface, thus the patterns for the two models are identical. In the third interval the surface angle first increases and then decreases when the streak enters the layer. This results in a higher peak in the volume flux curve since the total flux into the layer is higher due to rotation of the interface: when β_u decreases the flux from the bed into the layer is higher since $\omega_{\text{eff}} > \omega$ (see Eqs. (26) and (27)). The maximum in the volume flux curve is maintained at a high value due to this "pumping" by the interface motion. The maximum value of the volume flux falls if the critical composition (f_c) is chosen so that the interface is stationary (β_u constant). In the static interface model, the peak value falls with each passage of the streak through the layer, and eventually the streak is dissipated.

Consider next the formation of streaks starting with a radially segregated core formed at high rotational speed as in the experiments. Fig. 13 shows that streaks are indeed formed at the lowest rotational speed ($\omega = 0.75$ rpm). The parameters correspond to a mixture of 1 mm and 3 mm particles. In this case, choice of the critical composition (f_c) is very important. For all other parameters held fixed, we found a small specific range of values of f_c in which the flow in the lower half of the layer became time periodic. Fig. 14 shows the time variation of the surface angle (β_l) and the average composition (f_l) of the lower part of the layer for the first two half revolutions of the cylinder. This initial instability is the source of the streaks that grow with each passage through the layer. As the streaks grow, the value of the critical volume fraction is reduced to keep f_c close to the lower values of f_l. For

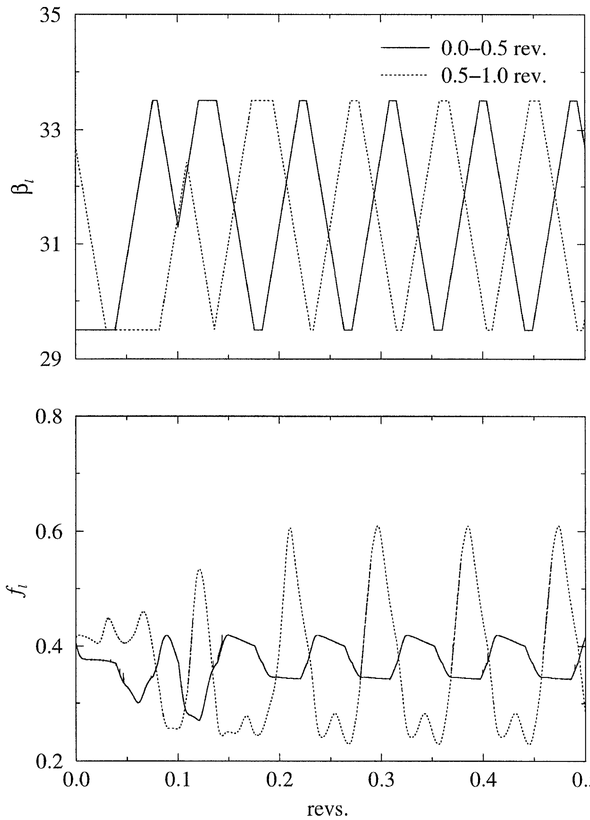

Fig. 14. Variation of the lower surface angle (β_l) and the average fraction in the lower part of the layer (f_l) with cylinder rotation for the first two half rotations of the cylinder computed using the moving interface model. The computations correspond to the initial condition and parameters of Fig. 13 for the 0.75-rpm case.

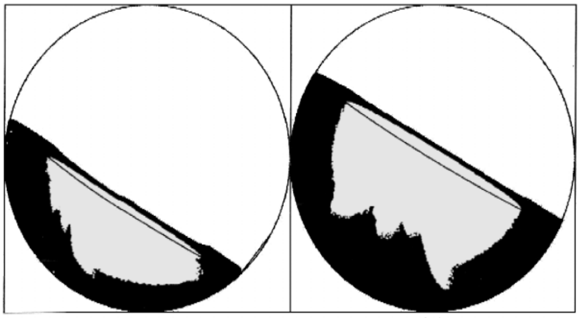

Fig. 15. Computed patterns formed after five revolutions for a cylinder rotational speed of 0.75 rpm. (a) Mixture of 3- and 1-mm beads at a fill fraction of 0.25. (b) Mixture of 3- and 2-mm beads at a fill fraction of 0.5.

example, in the computation of the results shown in Fig. 13, the values of the critical fraction used were: $f_c = 0.37$, 0.32, 0.26 and 0.23 in the first four half-revolutions, respectively. The core shrinks with the formation of streaks, hence the average concentration of small particles in the layer (when a streak is not passing through the layer) falls. Thus, f_c must be reduced to match the falling average concentration. If the value of f_c is not reduced, the streaks initially formed are eroded away.

Increasing the rotational speed to $\omega = 1.5$ rpm and putting $\delta_m = 0.02\,R$ to mimic the enhanced mixing in the layer, we get a reduction in the degree of streak formation. All other parameters are the same as those used for the 0.75-rpm case. Reducing the fill level to 25% for the low rotational speed case makes the streaks disappear (Fig. 15(a)). Finally, using a larger size ratio ($r_S = 2/3$) reduces the extent of streak formation (Fig. 15(b)). All these results are in qualitative agreement with experimental results. The dynamics of the model, however, are different from the experiments, and there are several quantitative differences. These differences arise from the very simple model used for the interface dynamics.

5. Conclusions

Two versions of a continuum model for flow and mixing of S-systems (binary mixture of large and small particles with the same density) are presented. In the first version, the dynamic variation of the flow in the layer due to concentration flow coupling and segregation are taken into account but the interface between the flowing layer and the bed is static. In the second version, the bed–layer interface is allowed to move in a simple prescribed manner depending on the local composition in the layer.

The static interface model does not produce streaks starting with a radially segregated configuration, even when parameters of the model are varied over a wide range. A constructed radial streak in the initial condition disappears with flow using the static interface model. In contrast, the moving interface model does give radial streak patterns starting from a radially segregated initial state. These results indicate the central importance to the motion of the interface driven by difference in angles of repose of the two flowing components. This conclusion is in agreement with the basis of the cellular automaton model of Makse et al. [15], which is the motion based on differences in angle of repose of the materials for producing streaks during heap formation. Computational results obtained indicate that an instability due to the coupling of the interface motion and flow in the layer may be the initiator of streaks. Computations also reveal a “pumping” mechanism due to interface motion, which may be responsible for the growth of streaks.

Results from experiments show that streak formation is suppressed by increasing rotational speed of the cylinder and by larger size ratios, r_S, that is smaller size differences. The streaks also disappear when the degree of filling becomes significantly less that half-full. The moving interface model makes qualitatively correct predictions of all these effects. The model for interface motion, in which the surface has rigid segments pivoted at two points, however, gives only a rudimentary description of the motion of the bed–layer interface. As a consequence, model predictions do not conform quantitatively to experimental results.

The level of complexity of the model is considerable. Improvements are undoubtedly possible and several modifications and improvements designed to increase the “degree of realism” of the model come to mind. The possible dynamical behavior of the model is explored only in the barest of details here. A more complete account of this behavior would most definitely require a self-contained study of these aspects alone. This, however, is only part of possible outcomes of pattern formation in S-systems. This becomes evident when changes in the driving mechanism are considered. Consider for example the case when the container shape is changed, and chaotic advection becomes possible. This should result in a wealth of possible outcomes resulting form the balance of chaos and ordering.

If anything, the most transparent way to explore all these aspects is to go to simpler models that nevertheless capture the essential elements of this picture. However, before this level of physical simplicity is reached, more studies analyzing the behavior of this, rather complicated model, seem to be called for.

Nomenclature

c	Collisional viscosity parameter (Eq. (20))
d_A, d_B	Particle diameters of small and large components
f	Average number fraction of small particles in the layer
f_c	Critical composition for up or down motion of interface

f_u, f_l Average number fraction of smaller particles in the upper and lower parts of the layer in the moving interface model
H Distance of free surface from cylinder axis (Fig. 1)
L Half-length of free surface (Fig. 1)
q Volume flux in the layer
R Cylinder radius (Fig. 1)
$r_S = d_A / d_B$ Size ratio
u_A, u_B Velocity profile parameters (Fig. 2)
v_x, v_y Velocity components in the layer (Fig. 1)
v_{Ax}, v_{Ay} Velocity components of the smaller particles in the layer
x_c Pivot point of moving interface (Fig. 3)

Greek letters
β Dynamic angle of repose (static interface model, Fig. 1)
β_A, β_B Dynamic angles of repose for the smaller and larger particles
β_{sA}, β_{sB} Static angles of repose for the smaller and larger particles
β_u, β_l Free surface angles of the upper and lower parts of the surface in the moving interface model (Fig. 3)
δ Layer thickness (Fig. 1)
δ_m Thickness of mixed zone in layer
ε Composition for transition in calculation of interface stress (Eq. (20))
ρ Bulk density of particles in the layer
ρ_A, ρ_B Mass densities of the smaller and larger particles in the layer
ρ_p Density of particles
ω Rotational speed of cylinder
ω_i Rotational speed of moving interface
ω_{eff} Local effective rotational speed taking into account interface motion

Symbols
$\langle . \rangle$ Average across the layer (Eq. (7))

Acknowledgements

This work was supported in part by grants to J.M. Ottino from the Division of Basic Energy Sciences of the Department of Energy. D.V. Khakhar acknowledges partial financial support of this work by the Department of Science and Technology, India through the award of the Swarnajayanti Fellowship (DST/SF/8/98).

References

[1] J. Duran, Sands, Powders and Grains. An Introduction to the Physics of Granular Materials, Springer-Verlag, New York, 2000.
[2] K.M. Hill, D.V. Khakhar, J.F. Gilchrist, J.J. McCarthy, J.M. Ottino, Segregation-driven organization in chaotic granular flows, Proc. Natl. Acad. Sci. 96 (1999) 11701–11706.
[3] T. Shinbrot, F.J. Muzzio, Nonequilibrium patterns in granular mixing and segregation, Phys. Today 53 (2000) 25–30.
[4] J.M. Ottino, D.V. Khakhar, Mixing and segregation of granular materials, Annu. Rev. Fluid Mech. 32 (2000) 55–91.
[5] J.T. Jenkins, F. Mancini, Kinetic theory for binary mixtures of smooth, nearly elastic spheres, Phys. Fluids A 1 (1989) 2050–2057.
[6] M.L. de Haro, E.G.D. Cohen, J.M. Kincaid, The Enskog theory for multicomponent mixtures: I. Linear transport theory, J. Chem. Phys. 78 (1983) 2746–2759.
[7] O. Walton, Proceedings of the DOE/NSF Workshop on Fluid–Solid Transport, Pleasanton, CA, May 1989.
[8] B.Ö. Arnarson, J.T. Willits, Thermal diffusion in binary mixtures of smooth nearly elastic spheres with and without gravity, Phys. Fluids 10 (1998) 1324–1328.
[9] T. Boutreux, P.G. deGennes, Surface flows of granular mixtures: I. General principles and minimal model, J. Phys. I 6 (1996) 1295–1304, France.
[10] S.B. Savage, C.K.K. Lun, Particle size segregation in inclined chute flow of cohesionless granular solids, J. Fluid Mech. 189 (1988) 311–335.
[11] S.S. Hsiau, M.L. Hunt, Granular thermal diffusion in flows of binary-sized mixtures, Acta Mech. 114 (1996) 121–137.
[12] D. Hirschfeld, D.C. Rapaport, Molecular dynamics studies of grain segregation in a sheared flow, Phys. Rev. E 56 (1997) 2012–2018.
[13] D.V. Khakhar, J.J. McCarthy, J.M. Ottino, Mixing and segregation of granular materials in chute flows, Chaos 9 (1999) 594–610.
[14] J.A. Drahun, J. Bridgwater, The mechanics of free surface segregation, Powder Technol. 36 (1983) 39–53.
[15] H.A. Makse, S. Havlin, P.R. King, H.E. Stanley, Spontaneous stratification in granular mixtures, Nature 386 (1997) 379–381.
[16] L. Prigozhin, H. Kalman, Radial mixing and segregation of a binary mixture in a rotating drum: model and experiment, Phys. Rev. E 57 (1998) 2073–2080.
[17] J.P. Koeppe, M. Enz, J. Kakalios, Phase diagram for avalanche stratification of granular media, Phys. Rev. E 58 (1998) R4104–R4107.
[18] J.J. McCarthy, T. Shinbrot, G. Metcalfe, J.E. Wolf, J.M. Ottino, Mixing of granular materials in slowly rotated containers, AIChE J. 42 (1996) 3351–3363.
[19] P.C. Johnson, R. Jackson, Frictional–collisional constitutive relations for granular materials, with application to plane shearing, J. Fluid Mech. 176 (1987) 67–93.
[20] J. Rajchenbach, Flow in powders: from discrete avalanches to continuous regime, Phys. Rev. Lett. 65 (1990) 2221–2224.
[21] M. Nakagawa, S.A. Altobelli, A. Caprihan, E. Fukushima, E.K. Jeong, Non-invasive flows of granular materials by magnetic resonance imaging, Exp. Fluids 16 (1993) 54–60.
[22] J. Rajchenbach, E. Clement, J. Duran, Experiments in model granular media: a study of gravity flows, in: F. Family, P. Meakin, B. Sapoval, R. Wool (Eds.), Fractal Aspects of Materials, 1995, p. 525, MRS Symposium, Pittsburgh.
[23] N. Jain, R.M. Lueptow, J.M. Ottino, Particle tracking techniques for measuring granular flows, in preparation, 2000.
[24] D.V. Khakhar, J.J. McCarthy, T. Shinbrot, J.M. Ottino, Transverse flow and mixing of granular materials in a rotating cylinder, Phys. Fluids 9 (1997) 3600–3614.